A THREE-DIMENSIONAL MODEL OF HAIL VOLUMES IN THE ATMOSPHERE AS EXTRAPOLATED FROM SURFACE MEASUREMENTS

T. R. Nicholas
National Hail Research Experiment
National Center for Atmospheric Research*
Boulder, Colorado

Abstract

Measurements of hail at the ground using a horizontal styrofoam impact surface have been used to evaluate the effect of cloud seeding on the mass of hail by the National Hail Research Experiment (NHRE). These point measurements of hail at the ground might usefully be augmented by weather radar measurements. In particular, radar can be used to interpolate between the point ground instruments and an overall integrated picture of the hail characteristics can be obtained. But in order to check the interpolation by comparing specific values taken from a square foot on the ground to a volume of atmosphere measured by radar which is on the order of a cubic kilometer substantial assumptions about hail trajectories need to be made. The numerous interrelated parameters associated with falling hail that enter this problem lend themselves readily to dynamic simulation by computer. A simple model of hail falling from cloud base being intercepted by a horizontal surface is presented with modular complexities such as horizontal and vertical wind fields, initial particle size distributions, melting and particle generation in the volume aided and their contributions evaluated. The aim of the simulation is to determine the effect of sampling a very small (1 ft^2) portion of the area of the hailfall under the various influences. Processes such as size sorting due to winds affect the validity of surface measurements if the sampling area is too small. Limited theoretical results are presented at this time with field-generated data providing boundary conditions and primary inputs.

Introduction

Hail and Surface Hail Measurements

Damage and destruction of crops in this country by hail account for substantial losses to the agricultural community. In 1973, the estimated annual loss from hail totalled more than 660 million dollars and that figure is still rising. To combat the problem, the National Science Foundation, through the National Center for Atmospheric Research (NCAR), has established the National Hail Research Experiment (NHRE) to study hailstorm mechanisms and to determine the feasibility of suppressing the damaging effects of hail by cloud seeding. Because hail storms are highly complex and ill-defined systems involving a number of microphysical and dynamical processes, they are very difficult to study in detail. The NHRE employs numerous data-gathering systems to aid its understanding of severe storms. Weather radar, research aircraft, and surface precipitation instruments all contribute independent measurements of storm characteristics. Yet, even the most advanced instruments suffer from limitations such as their small sampling area compared to the enormous extent of storms and their spatial variability of hailfall. In order to develop measuring systems which are sensitive to possibly small effects of seeding, a great deal must be known about the natural precipitation processes and about instrument capabilities. Spatial variability of hailfall as measured at the ground is of major concern to this presentation since it is there that the damaging effect of hail is felt.

Hail Instrumentation - The Hailpad

The ground measurement system presently used consists primarily of an array of impact-sensitive hailpads, examples of which are shown in Figure 1. The pad consists of a foil-covered styrofoam pad which retains an impression of a hail impact on its surface. Through calibration, the measurement of the dimensions of a dent yields the size of a hailstone from which a time integrated hailstone size distribution is calculated. By making assumptions about the shape, hardness, density and composition of the stones, as well as the spatial variability of hailfall and wind effects, such parameters as total impact momentum, energy and mass can be derived (1). The assumptions are substantial, however, and affect the accuracy of the derived parameters. Actual measurement of such hail characteristics as impact angle and direct measurements of energy or momentum are considerably better, but costs are greatly increased (2).

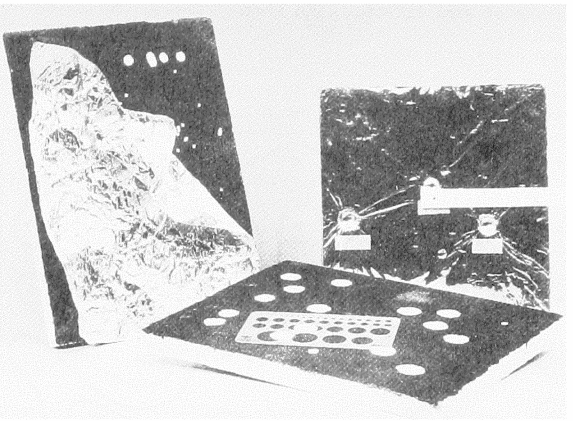

Figure 1 NHRE hailpads shown with aluminum foil coverings and circle template used for digitizing indentations. Dents are highlighted by roller painting the surface.

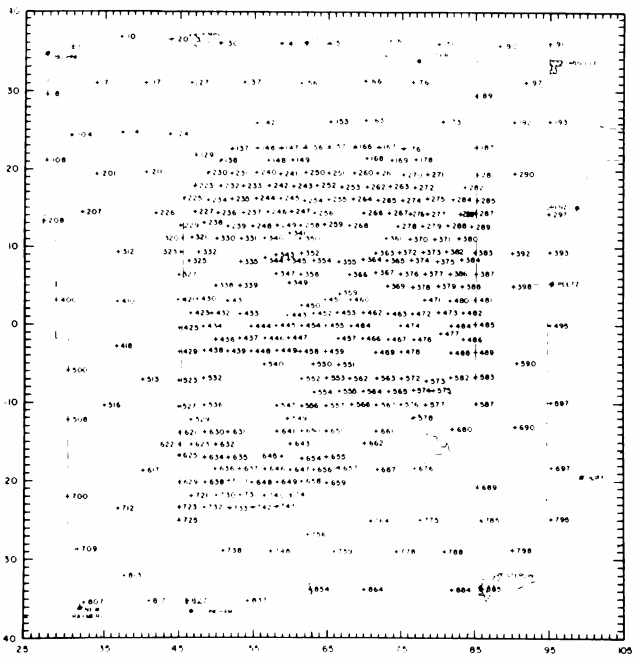

Figure 2 NHRE surface precipitation network. Numbers identify instrument locations. Densely instrumented core is the experimental target area. Scale is in kilometers.

* This research was performed as part of the National Hail Research Experiment, managed by the National Center for Atmospheric Research and sponsored by the Weather Modification Program, Research Applications Directorate, National Science Foundation.

In spite of the advances in instrumentation, there remains a substantial question about the adequacy of sampling area of most systems for the direct measurement of hail. Figure 2 illustrates the arrangement of the NHRE's surface hail instrumentation in and around the "target area" located in Northeast Colorado. Within the densely-instrumented target area, spacing is approximately one instrument every two kilometers. In the buffer area, it is one-fifth that density. Each instrument samples roughly one-tenth of a square meter. This results in a sampling ratio of 5×10^{6}. A study of the spatial variation of hail in 1973 (3) yielded figure 3. Within a square mile were placed 90 hailpads and hail "cubes," the latter designed to measure hail size distributions and to give an estimate of wind effects. The figure shows a 10-fold variation over the square mile in the number of stones per square meter measured. Similar variations were found between adjacent pads. It was concluded that even this dense network was inadequate to confidently measure hail patterns due to the extreme variability of the hail.

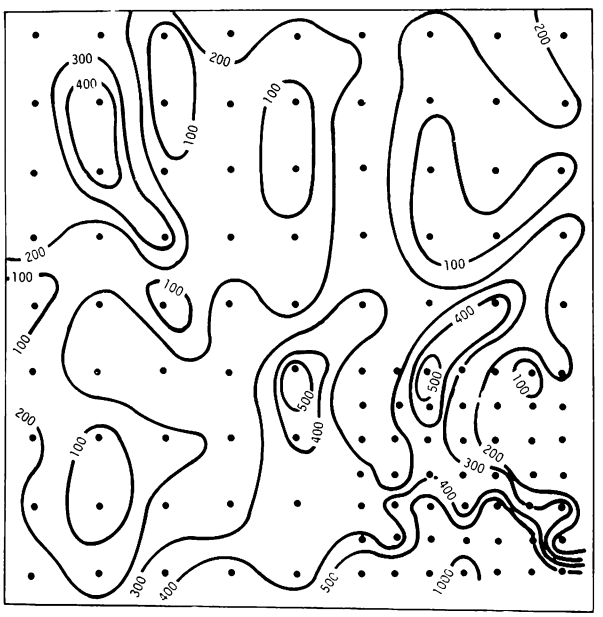

Figure 3 Distribution of the total number of hailstones per square meter from one square mile, 21 May 1973. Dots represent instrument locations.

Changnon (4) has indicated that on the average, a hail "streak" has dimensions 2 km by 7 km and can have many smaller "cores" of high intensity hail within it. Thus, a hailfall generally covers a large area in very non-uniform patterns. The combined measuring requirements of large extent and high sampling density appear to present insurmountable obstacles for adequate measurement of hail at the ground. There are, however, complementary measurements of hail using radar that can be implemented. Computer simulation can help determine optimum sampling density and extent of a network of surface instruments. It is the complementary employment of three systems, radar, surface network and computer model, which is the subject of this paper.

The Research Radar

Recent developments in the area of weather radars have provided the first quantitative representation of the three-dimensional structure of flow patterns within a storm. Using a system developed by the National Oceanic and Atmospheric Administration's (NOAA) Wave Propagation Laboratory (WPL), scientists scan a storm with two S-band Doppler radars simultaneously. This coplanar scan allows subsequent derivation of three-dimensional Doppler spectra in the intersection of the two beams (5).

Figure 4 schematically represents the coplanar scan scheme and shows that the data reduces to (u,v,w) components of air motion in addition to reflectivity factor at about 1/2 km grid points. Reflectivity factor is a number representative of the number concentrations of water and ice particles in the radar illuminated volume. Using the reflectivities and assumptions about the mean particle fall velocity which will be discussed later, three-dimensional components of air motion can be derived from the Doppler velocities of the two radars. From the air motions large scale size sorting of particles in a storm can be studied and trajectories of particles falling through the air flow field can be predicted. These studies will provide a link between the observed particle concentrations in the cloud and the measured precipitation at the ground.

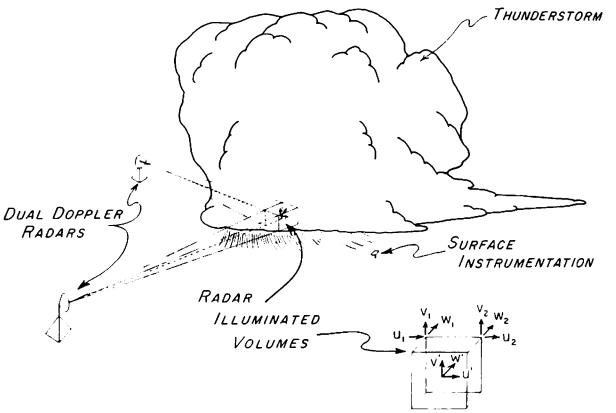

Figure 4 Schematic representation of dual Doppler radar coplanar scan. The illuminated volume (inset) shows three-dimensional air velocities at grid points from the radars (u_1, v_1, w_1), (u_2, v_2, w_2) and an interpolated value within the volume (u', v', w').

Mathematical Modeling

To bridge the gap between radar measurements and the surface precipitation measurements requires knowledge of or predictions for the trajectories of different size particles under the influence of air motions. Predictions have been obtained by construction of a kinematic model of particles falling from cloud base to ground through measured air flow fields. In the model, the particles move in response to the air motion and gravity and also shrink in size due to melting and evaporation. At the surface such parameters as final stone size, traverse time, and angle, velocity, momentum and energy of impact are calculated. The positions calculated at the surface predict the final arrangement of the precipitation particles which have been measured by the surface instrument network.

The Model

Initial conditions: Particles passing through the horizontal plane at cloud base enter the system with an initial position and size. From the radar reflectivity factors measured at cloud base, an exponential particle size distribution at each grid point can be deduced. The data from the dual Doppler radars includes both reflectivity factors and estimates of mean particle fall velocities as calculated from an empirical relationship derived by Joss and Waldvogle (6).

$$\langle v \rangle = 2.6Z^{.107} \qquad (1)$$

where: $\langle v \rangle$ = the mean Doppler velocity (m/sec)

Z = the reflectivity factor in $mm^6\ m^{-3}$

From the mean velocity the median particle diameter can be estimated from equations presented by Atlas, Srivastava and Sekhon (7).

The mean Doppler Velocity is defined by:

$$\langle v \rangle = \int_o^\infty v Z_v'(v)\, dv / \int_o^\infty Z_v'(v) dv \qquad (2)$$

where: $\langle v \rangle$ = mean Doppler velocity (m/sec)

v = particle fall velocity (m/sec)(see below)

$Z_v'(v)$ = Doppler spectrum corresponding to the radar reflectivity factor (mm^6/m^3) $(m/sec)^{-1}$

by definition:

$$Z_v'(v)dv = N_D(D)D^6 dD \qquad (3)$$

where: $N_D(D) = N_o e^{-\Lambda D}$, N_o and Λ are parameters of the exponential particle size distribution

D = particle diameter (cm)

Using the relationship from Gunn and Kinzer (8):

$$v = a_1 - a_2 e^{-bD} \qquad (4)$$

where: v = fall velocity cm/sec

$a_1 = 965$

$a_2 = 1030$

and integrating equation (2) results in:

$$\langle v \rangle = 965 - 1030 [\Lambda/(\Lambda+6)]^7 \text{ (cm/sec)} \qquad (5)$$

from which the slope of the exponential particle size distribution Λ is calculated. Then, from the definition of the reflectivity factor Z:

$$Z = N_o \int^\infty e^{-\Lambda D} D^6 dD \qquad (6)$$

Assuming an exponential size distribution as above and integrating yields the exponential intercept N_o:

$$N_o = \frac{Z \Lambda^7}{720} \qquad (7)$$

A lengthy discussion of the assumptions and error sources involved in the previous derivation is beyond the scope of this presentation. It is important to note, however, that in the presence of hail, equation (1) may be in error somewhat. The effect of this is lessened somewhat by the small exponent in (1). Empirical equations similar to these are now being developed for situations where hail is present. The initial conditions are defined at grid points with 0.5 km spacing at cloud base; particle size distributions are generated at these points.

A realistic spatial distribution of particles at cloud base is not the only initial condition system which can be applied to the model. Simpler initial conditions can be used to determine the effects of the flow fields and the microphysics on particle trajectories. For instance, particles of the same size can be introduced into different parts of the storm and the effect of initial position on their relative final positions noted. Similarly, particles of different sizes can be introduced at the same point and the effect of size sorting studied. Two examples of model output, discussed later, used such simple initial conditions.

Forces: A particle moves under the influence of gravity and drag while falling unhindered through the atmosphere. The combination of gravity and drag forces determines the terminal velocity a particle of a given size, shape, mass and composition will attain in free fall. Nearly all hailstones and raindrops falling through the atmosphere will be in the Newton's flow range defined by the following equation from McCabe and Smith (9):

$$U_t = \left(\frac{4\, g\, D_p (\rho_p - \rho)}{3\, C_D\, \rho} \right)^{1/2} \qquad (8)$$

where: U_t = terminal velocity (cm sec^{-1})

g = acceleration of gravity = 980.16 (cm sec^{-2})

D_p = particle diameter (cm)

ρ_p = particle density = .91(g cm^{-3}) for ice; 1 (g cm^{-3}) for water

C_D = drag coefficient ($\sim$ .44 for spheres)

ρ = air density (g cm^{-3})

The density of moist air from the CRC Handbook of Physics (10) varies with pressure and temperature in the following manner:

$$\rho = .001293 \left(\frac{273.13}{T} \right) \left(\frac{P - .3783\, e}{760} \right) \qquad (9)$$

where: ρ = density of moist air (g cm^{-3})

T = temperature (°K)

P = atmospheric pressure (mm Hg)

e = vapor pressure (mm Hg)

From Hess (11) the vapor pressure is calculated as follows:

$$e = \left(\frac{RH \cdot P}{\frac{e_s}{1} + RH} \right) \qquad (10)$$

where: RH = atmospheric relative humidty * .01

P = atmospheric pressure (bars)

e_s = saturation vapor pressure (bars)

From Murray (12):

$$e_s = 6.1078 \times 10^{-3} \exp \left(\frac{17.269\, T}{237.3 + T} \right) \qquad (11)$$

where: e_s = saturation vapor pressure (bars)

T = atmospheric temperature (°C)

The particles are assumed to instantaneously assume the speed of horizontal and vertical air motions. This is reasonable for currents of a size which could significantly affect the direction of fall of the particle. Pressure, temperature and humidity profiles for a particular day are obtained from rawinsonde data near the area of interest. The atmosphere below cloud base is assumed to be unaffected by previous cooling and humidification by falling precipitation. The hailstones are assumed to be smooth, hard spheres of constant, .91 g/cm^{-3} and homogeneous density.

Melting and Evaporation: Mason (13) shows that a hailstone which falls from frozen regions in a cloud into the warmer air below shrinks by melting and shedding water from its surface according to the following equation:

$$\frac{dr}{dt} = \left(\frac{1}{8} \frac{x\, R_e^{1/2}}{L_f\, \rho_p\, r} \right) \left(Lv\, D\, (\rho_v - \rho_o) + K(T_w - T) \right) \qquad (12)$$

where: r = particle radius (cm)

t = time (sec)

x = ventilation factor (for spheres = .68)

R_e = Reynolds number = $\left(\frac{2\, r U_t \rho}{\mu} \right)$

μ = viscosity of air

$= 1.8325 \times 10^{-4} \left(\frac{416.16}{T + 120.} \right) \left(\frac{T}{296.16} \right)^{3/2}$ (poise)

L_f = latent heat of fusion = 79.7 (cal g^{-1}) at 0°C

ρ_p = particle density (g cm^{-3}) = .91 for ice

L_v = latent heat of vaporization (cal g^{-1})

$= 597.3 - .566\, T$ (with T in °C)

D = diffusivity of water in air

$= .226 \left(\frac{T}{273.16}\right)^{1.81} \left(\frac{1000}{P}\right)$

with T in °K, P in mb ($cm^2\ sec^{-1}$)

ρ_v = saturation vapor density at 0°C

$= 4.84 \times 10^{-6}$ ($g\ cm^{-3}$)

ρ = air density ($g\ cm^{-3}$)

K = thermal conductivity = $.578\mu$ ($cal\ cm^{-1}\ sec^{-1}\ °K^{-1}$) with μ in poise

T_s = temperature at surface of stone = 273.16°K

T = ambient temperature (°K)

Once a melting stone reaches 5mm diameter the melting shedding process is replaced by an evaporation process. This transition point is based on observations which show relatively few natural raindrops larger than 5 mm diameter. The evaporation equation from Mason (13) is:

$$\frac{dr}{dt} = \frac{\sigma\left(1 + F\,Re^{\frac{1}{2}}\right)}{\left(\frac{r\,L_v^2\,\rho_l}{RKT^2}\right) + \left(\frac{R\,T\rho_l}{D\,e_s}\right)} \qquad (13)$$

where: σ = subsaturation of the atmosphere

$= \left(\frac{RH\ P}{e_s(RH-1)+P}\right)^{-1}$

with RH = relative humidity of atmosphere (x.01)

P = atmospheric pressure (bars)

F = ventilation factor = .23

R = specific gas constant for water = .11033 ($cal\ g^{-1}\ °K^{-1}$)

e_s = saturation vapor pressure ($cal\ cm^{-3}$)

Air Motions: The three-dimensional air flow fields which have been derived from the dual Doppler radar data move the particles in three dimensions as they fall. The assumption is made that the particle accelerates to the speed of the air motion instantaneously. The Doppler data consists of cartesian components of air velocity (u,v,w). Overall storm motion is included in the data and must be allowed for. The velocity components are presented at cartesian grid points relative to the radar origin (a point half way between the two radars) with a typical spacing of 500 m. Figure 5 shows u-w wind vectors on an X-Z plane taken through a storm of interest. The length of the vector is proportional to its magnitude. The entire grid is assumed to have been generated at the same time even though a sweep sequence may take two to three minutes. Each sweep is assigned a time at the start of the scan. A three-dimensional linear interpolation scheme is used to derive u', v', and w' components at points other than grid points (see figure 4). For values between scans, the last known sequence is used until it is replaced by a new scan. Interpolation in the time domain yields misleading results because of the variable scan patterns used. No attempt is made to smooth or filter the data prior to interpolation since the grid values are pre-filtered in the data reduction and the grid is coarse relative to scales of turbulence which are of interest.

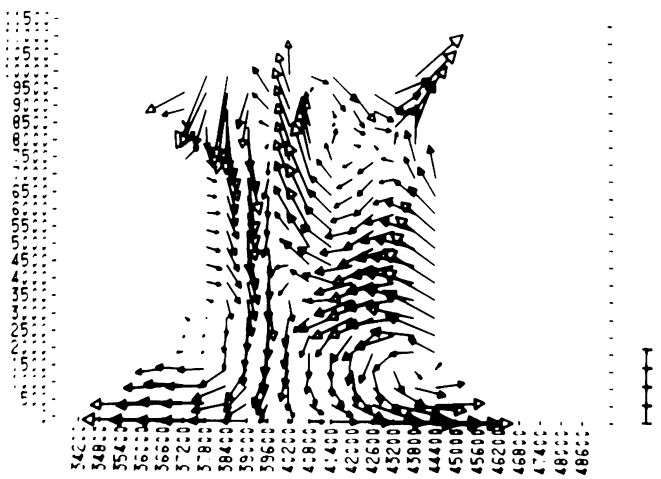

Figure 5 Vector diagram from dual Doppler radars 28 July 1973 storm. Shown is an X-Z plot of two-dimensional flow fields in an east-west orientation. Vector lengths shown at lower right correspond to 5m/sec. Axes are in meters.

The Differential Equations: Four linear, first order ordinary differential equations describe the trajectory of a falling particle:

$$\frac{dx}{dt} = U(X,Y,Z,t) \qquad (14)$$

$$\frac{dy}{dt} = V(X,Y,Z,t) \qquad (15)$$

$$\frac{dt}{dt} = W(X,Y,Z,t) - U_t \qquad (16)$$

$$\frac{dr}{dt} = \text{Expressed in eq. (11), (12)}$$

where: X,Y,Z = cartesian position variables (m)

t = time (sec)

U,V,W = cartesian velocity variables ($m\ sec^{-1}$) North, East and up directions are assumed positive.

U_t = terminal fall velocity ($m\ sec^{-1}$)

r = particle radius (cm)

The Integration Scheme: The method chosen for digital integration of these equations is the Adams-Moulton 4th order predictor-corrector method. It was chosen for its stability even though the equations tend to be very tame. The variable time step allows for very efficient integration.

Output Parameters: The output from the simulation consists of digital time-position data, final impact parameters, and a three-dimensional mapping of the trajectory. The impact parameters are the particle size, its position relative to its origin, its traverse time, the impact angle, velocity, momentum and energy and its phase (solid or liquid). Impact velocity is simply the vector sum of the final velocity components. The impact momentum and energy are given by:

$$P = MV \qquad (17)$$

and

$$E_k = \tfrac{1}{2}M\,V^2 \qquad (18)$$

where: P = momentum (nt-sec)

M = mass (g)

V = resultant velocity ($m\ sec^{-1}$)

E_k = kinetic energy (Joules x 10^{-7})

The impact angle (measured from the vertical) is:

$$\Theta = \text{Tan}^{-1}\left(\frac{U^2 + V^2}{|W|}\right) \qquad (19)$$

A sample three-dimensional map of trajectories is shown in figure 8. All axes are in meters and the numbers near each trace indicate the particle number corresponding to digital output which is summarized in Table 1. If the particle has melted during its fall, a note to that effect is included with the digital output.

The Computer: The simulation is run on a Control Data Corporation 7600 computer belonging to NCAR. The program uses 45,000 words of memory and one trajectory plots in about three seconds CPU time. The graphical output is photographed by microfilm camera attached to the system.

28 July 1973: On 28 July 1973 in the NHRE target area of Northeast Colorado, a storm was observed by dual-Doppler radars for ten minutes during its mature stages. Figure 6 shows contoured radar reflectivities of the storm at 1718 MDT when the first scan sequence was taken. The figure also shows ten-minute positions of the centroid of maximum reflectivity tracking to the southeast. Other measuring systems also produced information about the storm. A rawinsonde balloon was launched at 16:20 MDT from Sterling, Colorado, fifteen miles south of the storm. From the sounding, height-dependent temperature, pressure and humidity of the undisturbed atmosphere are applied to the model for calculations of particle melting and evaporation. Under the storm, precipitation gauges measured up to 3 cm of rain as the storm passed giving timed records of the actual rainfall rates.

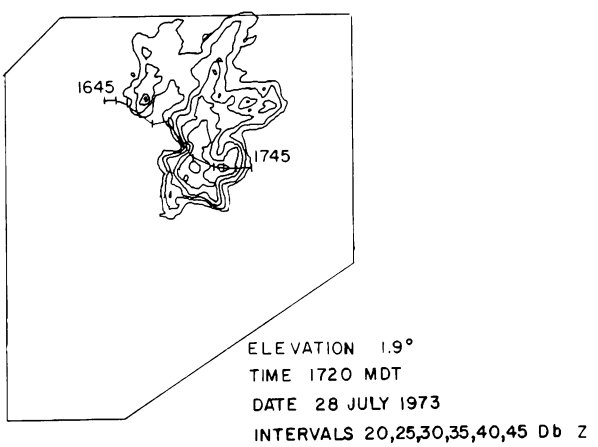

Figure 6 Radar contoured reflectivity factors of 28 July 1973 storm at 1720 MDT. Contour levels, radar beam elevation and time data are shown. The border outlines the target area boundary (see Figure 2). Hatch marks trace the centroid of maximum reflectivity at ten-minute intervals from 1645 to 1745 MDT.

Evaluation of the radar reflectivities indicates that little hail was present in this storm. This is borne out by the ground hail sensors which recorded only sporadic amounts of small hail. Other case studies, now being analyzed, contain more evidence of hail and should lend to a more intensive study of hailstone trajectories.

Sample Output: To illustrate the capabilities of the model two examples of relative particle trajectories are presented as figures 7 and 8. Figure 7 illustrates the effect of sorting on five particles of different initial sizes that fall from the same point through the air motion field measured on 28 July 1973 starting at 1718 MDT.

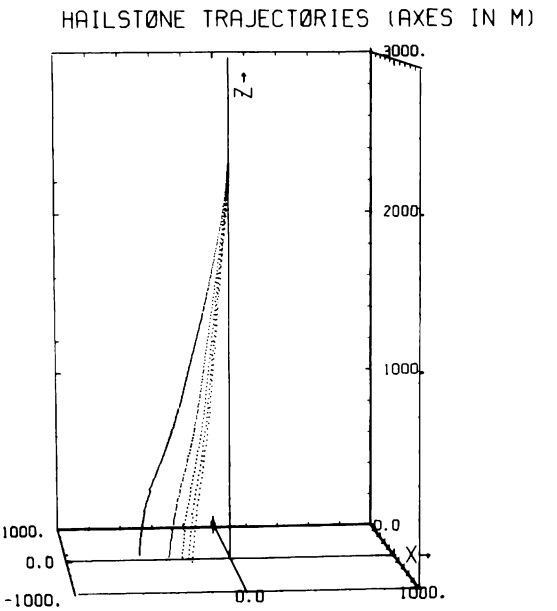

Figure 7 Three-dimensional computer-generated plot of trajectories of five particles released at z = 2400 m (cloud base) and falling through dual Doppler radar-generated air flow fields. Axes are in meters, origin corresponds to the location of raingauge 364 in the NHRE network. Each dot corresponds to a one-second position. Particle sizes are 0.5, 1.0, 1.5, 2.0, 2.5 cm radius with the larger particles falling closer to the origin.

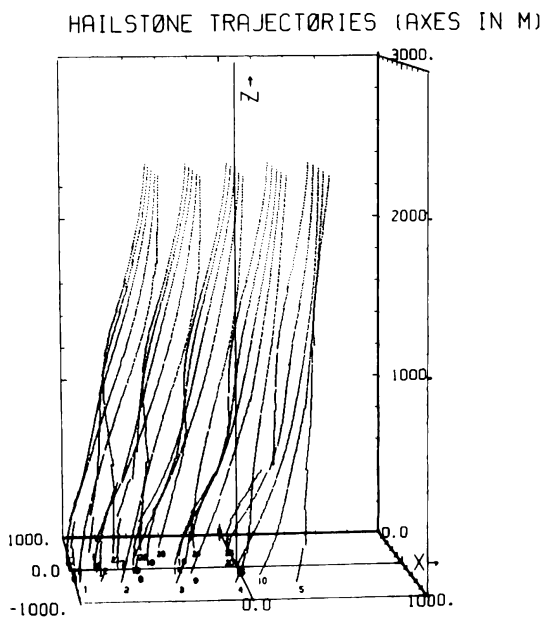

Figure 8 Three-dimensional computer-generated plot of trajectories of twenty-five 0.5 cm radius particles released at 1/4 km intervals at cloud base. Axes are in meters. Each dot corresponds to a one-second position and the numbers below each trajectory termination point identify the particle and correspond to a set of computations presented on the digital output.

Figure 8 shows the paths of 25 particles initially 1 cm diameter falling from a 1 km square area. All the particles had melted by the time they reached the ground. Travel times from cloud base (2400 m) to the ground varied from 191 seconds to 215 seconds and the sizes of particles hitting the ground varied from .42 to .50 cm diameter as shown in Table 1. Trajectories ofthe particles shows strong flow from east to west and some north-south divergence. Some particles traveled nearly a kilometer laterally during their fall of 2.4 km, though impact angles which relfect only local mean air motions vary from 2 to 34 degrees from the vertical.

The model volume was placed in the storm over a ground raingauge which recorded about 75 mm/hr rainfall rate for the period of interest.

The line of data in Table 1 with an asterisk shows that the particle which most nearly hit the raingauge, located at the origin, started 1/2 km to the east at cloud base. This indicates that for 1 cm diameter particles which contributed to the measured precipitation, the cloud-base origin was 500 m east and somewhat north of the instrument.

Discussion

The sample output presented above illustrates the capabilities of the model. Comprehensive results are not yet available. In process is a calculation of particle size distribution parameters from radar reflectivities measured at cloud base. Using the distributions calculated at grid points and broken into discrete size categories, trajectories of particles generated in the 300 meter space surrounding each grid point are being traced. The number of particles equal to that computed for the size range at its origin are assigned to each trajectory and the result is a theoretical spatial size distribution of particles at the ground. The generated spatial distribution is then related in time to ground measurements of precipitation. Finally, using empirical relations between precipitation rate and reflectivity factor and measured precipitation rates, verifications of measured reflectivity factors are made. The aim of this analysis is to establish the effectiveness of using radar reflectivity measurements to predict precipitation intensity at the ground by interpolating between surface measurements.

Radius		Traverse Time	X		Y		Z		Impact Angle	Impact Velocity	Impact Momentum	Impact Energy	Final State	
Initial (cm)	Final (cm)	(sec)	Initial (m)	Final (m)	Initial (m)	Final (m)	Initial (m)	Final (m)	(Deg)	(m/sec)	(Nt-sec)	(Joules)	(M=melted)	
.5	.25	191	0.0	-609.2	0.0	196.5	2400.	0.0	6	10.4	6.32×10^{-4}	3.25x10-3	M	
1.0	.6	118	0.0	-360.2	0.0	117.2	2400.	0.0	6	16.3	1.368×10^{-2}	1.108×10^{-1}		
1.5	1.2	92	0.0	-283.7	0.0	93.6	2400.	0.0	6	23.2	1.65×10^{-1}	1.91×10^{0}		
2.0	1.8	79	0.0	-247.3	0.0	80.6	2400.	0.0	6	28.0	6.08×10^{-1}	8.49×10^{0}		
2.5	2.3	71	0.0	-224.4	0.0	73.4	2400.	0.0	6	31.8	1.51×10^{0}	2.41×10^{-1}		
.5	.23	204	-500.	-937.2	-500.	-348.8	2400.	0.0	2	10.1	5.46×10^{-4}	2.75×10^{-3}	M	
.5	.23	203	-250.	-729.0	-500.	-374.5	2400.	0.0	15	10.2	4.94×10^{-4}	2.52×10^{-3}	M	
.5	.25	196	-0.0	-393.1	-500.	-400.9	2400.	0.0	27	11.6	7.32×10^{-4}	4.24×10^{-3}	M	
.5	.25	199	250.	- 47.2	-500.	-452.2	2400.	0.0	31	12.1	7.75×10^{-4}	4.69×10^{-3}	M	
.5	.21	212	500.	273.4	-500.	-455.7	2400.	0.0	32	11.1	4.02×10^{-4}	2.23×10^{-3}	M	
.5	.23	194	-500.	-1018.9	-250.	- 30.4	2400.	0.0	12	10.3	5.59×10^{-4}	2.87×10^{-3}	M	
.5	.22	197	-250.	-855.5	-250.	- 33.3	2400.	0.0	11	9.8	4.09×10^{-4}	2.01×10^{-3}	M	
.5	.24	190	0.0	-626.1	-250.	- 63.1	2400.	0.0	1	10.3	6.15×10^{-4}	3.15×10^{-3}	M	
.5	.23	194	250.	-293.1	-250.	-134.7	2400.	0.0	24	10.9	5.64×10^{-4}	3.08×10^{-3}	M	
.5	.24	197	500.	109.0	-250.	-193.2	2400.	0.0	34	12.2	6.93×10^{-4}	4.22×10^{-3}	M	
.5	.24	193	-500.	-983.0	0.0	188.0	2400.	0.0	13	10.4	5.82×10^{-4}	3.02×10^{-3}	M	
.5	.24	194	-250.	-804.3	0.0	210.3	2400.	0.0	13	10.4	5.94×10^{-4}	3.10×10^{-3}	M	
.5	.25	191	0.0	-609.2	0.0	196.5	2400.	0.0	6	10.4	6.55×10^{-4}	3.41×10^{-3}	M	
.5	.25	191	250.	-350.5	0.0	165.6	2400.	0.0	9	10.5	6.64×10^{-4}	3.47×10^{-3}	M	
.5	.25	190	500.	18.0	0.0	80.7	2400.	0.0	28	11.7	7.50×10^{-4}	4.40×10^{-3}	M	*
.5	.23	203	-500.	-838.0	250.	368.5	2400.	0.0	11	10.0	4.79×10^{-4}	2.41×10^{-3}	M	
.5	.23	203	-250.	-683.9	250.	410.3	2400.	0.0	10	10.1	4.97×10^{-4}	2.50×10^{-3}	M	
.5	.24	197	0.0	-509.8	250.	440.0	2400.	0.0	7	10.2	5.78×10^{-4}	2.95×10^{-3}	M	
.5	.24	196	250.	-311.9	250.	440.9	2400.	0.0	2	10.2	5.78×10^{-4}	2.94×10^{-3}	M	
.5	.22	196	500.	- 50.0	250.	394.0	2400.	0.0	12	10.0	9.61×10^{-4}	2.31×10^{-3}	M	
.5	.23	215	-500.	-714.2	500.	558.8	2400.	0.0	7	10.0	4.87×10^{-4}	2.43×10^{-3}	M	
.5	.22	213	-250.	-546.8	500.	622.9	2400.	0.0	8	9.9	4.56×10^{-4}	2.26×10^{-3}	M	
.5	.24	204	0.0	-376.6	500.	670.0	2400.	0.0	9	10.3	6.04×10^{-4}	3.12×10^{-3}	M	
.5	.23	205	250.	-194.6	500.	699.5	2400.	0.0	10	10.0	4.80×10^{-4}	2.41×10^{-3}	M	
.5	.23	200	500.	18.6	500.	695.6	2400.	0.0	5	10.0	4.95×10^{-4}	2.47×10^{-3}	M	

Table 1 Summary of sample data giving impact parameters and digital end points of trajectories corresponding to figures 7 and 8.

Using the spatial distribution of precipitation intensity generated by the model, an analysis of spatial variance of the precipitation relative to point measurements from a hypothetical network of instruments of varying sizes and numbers density is being performed. The result of this analysis is to determine an acceptable sampling area of a particular storm which will then help determine the optimum instrument sampling size and network extent and density.

Analysis of a storm with confirmed hail present will supply more useful information than the present case. Nonetheless, the analysis techniques employed will not change and this case provides a good check of the method since rain is generally a more well-behaved system than hail.

Acknowledgments

Credit is due to the NHRE staff and contributing contractors, especially NOAA's Wave Propagation Laboratory for advice, consultation and data for this paper.

References

1. Nicholas, T. R., "Surface Hail Instrumentation in the NHRE," Proceedings NHRE Symposium/Workshop on Hail, pp. VIII B.A. 1-38, Sept. 1975.

2. Changnon, Stanley A., Jr. and Donald W. Staggs, "Recording Hailgage Evaluation," Final Report for NSF Grant GA-1520, Illinois State Water Survey, Urbana, 47 pp., 1969.

3. Morgan, Griffith M., and Neil G. Towery, "Microscale Studies of Surface Hail," Final Report, NCAR 25-73, for UCAR, 35 pp., 1974.

4. Changnon, S. A., "Hailfall Characteristics Related to Crop Damage," J. Appl. Meteor., 10, 270-274, 1970.

5. Kropfli, R. A., and L. J. Miller, "Kinematic Structure and Flux Quantities in a Convective Storm from Dual Doppler Radar Observations," to be published in J. Appl. Sci., 33, March 1976.

6. Joss, J. and A. Waldvogel, "Raindrop Size Distribution and Doppler Velocities," Proceedings, 14th Radar Meteorology Conference, Amer. Meteor. Soc., Boston, Mass., Tucson, Ariz., Nov. 17-20, 1970.

7. Atlas, D., R. C. Srivastava, and R. S. Sekhon, "Doppler Radar Characteristics of Precipitation at Vertical Incidence," Reviews of Geophysics and Space Physics, 11, No. 1, pp. 1-35, Feb. 1973.

8. Gunn, R., and G. D. Kinzer, "The Terminal Velocity of Fall for Water Droplets in Stagnant Air," J. Meteor., 6, pp. 243-248, 1949.

9. McCabe, Warren L., and Julian C. Smith, Unit Operations of Chemical Engineering, 2nd Ed., McGraw-Hill Book Co., New York, pp. 166-169, 1967.

10. Weast, Robert C., ed., Handbook of Chemistry and Physics, 54th Ed., C. R. C. Press, p. F9, 1973.

11. Hess, Seymour L., Introduction to Theoretical Meteorology, 1st ed., Holt, Rinehart and Winston, New York, pp. 58-60, 1959.

12. Murray, F. W., "On the Computation of Saturation Vapor Pressure," J. Appl. Meteor., 66, pp. 203-205, Jan. 1967.

13. Mason, B. J., The Physics of Clouds, 2nd Ed., Clarendon Press, Oxford, pp. 312-366.